CrossMark

One-Minute Quasi-Periodic Pulsations Seen in a Solar Flare

Z. Ning[1] (ID)

Abstract We study quasi-periodic pulsations (QPPs) in the SOL2014-09-10 event that was detected by the *Geostationary Operational Environmental Satellites* (GOES), the *Atmospheric Imaging Assembly* (AIA) and the *Extreme Ultraviolet Variability Experiment* (EVE) onboard the *Solar Dynamics Observatory* (SDO), and the *Gamma Ray Burst Monitor* (GBM) onboard the *Fermi* satellite. Previous studies have found that this flare displays four-minute QPPs in a broad range of wavelengths. In this article, we find that this event also shows QPPs with a period of around one minute. Using the Fast Fourier Transform (FFT) method, the light curves are decomposed into fast- and slowly varying components with a separation at ≈ 100 seconds. The four-minute QPPs are in the slowly varying component, and the one-minute QPPs are identified with the fast-varying components in the impulsive and maximum phases. Similarly as the four-minute QPPs, the one-minute QPPs are simultaneously found in soft X-rays (SXR), extreme ultraviolet (EUV), and hard X-ray (HXR) emission. High correlations are found between the fast-varying components at the different wavelengths, especially between SXR and HXR. The spatial location of the sources of one-minute QPPs differ from those of the four-minute QPPs. The four-minute QPPs appear in the whole flare region, while the one-minute QPPs tend to originate from the flare loop footpoints. This finding provides an observational constraint for the physical origin of the QPPs.

1. Introduction

Observations show that some solar flares exhibit quasi-periodic pulsations (QPPs) or oscillations in their emissions. In a typical example, QPPs appear as regular and periodic peaks

✉ Z. Ning
   ningzongjun@pmo.ac.cn

[1] Key Laboratory of Dark Matter and Space Astronomy, Purple Mountain Observatory, Nanjing 210008, China

in the flare light curves over a broad wavelength range from the radio through visible, extreme ultraviolet (EUV), to soft and hard X-ray (SXR; HXR), and even γ-rays. Each peak has a similar profile, which results in a regular lifetime. Therefore, the QPPs are characterized by repetition or periodicity. Based on the observations, the periods of QPPs are usually split into several bands, such as short (subseconds) through medium (seconds) to long (minutes) (Aschwanden, 1987; Wang *et al.*, 2002; Karlický *et al.*, 2005; Nakariakov, 2007; Fleishman, Bastian, and Gary, 2008; Sych *et al.*, 2009; Nakariakov *et al.*, 2010a, 2010b; Kupriyanova *et al.*, 2010, 2014; Tan, 2010; Van Doorsselaere *et al.*, 2011; Nakariakov and Zimovets, 2011; Ning, 2014; Simões, Hudson, and Fletcher, 2015). Previous studies showed that the various periods might be related to different physical processes. For example, QPPs with a subsecond (short) period are often detected in light curves at the radio and HXR emissions thanks to the high temporal resolution (Aschwanden, 1987; Aschwanden *et al.*, 1994; Fleishman *et al.*, 2002; Ning *et al.*, 2005, 2007). They are thought to be related with kinetic processes caused by the dynamic interaction between plasma waves and energetic electrons trapped in the flaring loops (Aschwanden, 1987). QPPs with a medium period at tens of seconds and minutes are detected over a wide wavelength range from microwave, EUV, SXR and HXR, also even γ-rays. They might be associated with the magnetohydrodynamic (MHD) processes not only in the flaring loops (Aschwanden *et al.*, 1999; Nakariakov *et al.*, 1999; De Moortel *et al.*, 2002; Wang *et al.* 2002, 2003; Kliem *et al.*, 2002; Ofman and Wang, 2002; Su *et al.*, 2012a, 2012b; Yuan *et al.*, 2015), but also in more complex magnetic configurations that appear in the flare regions, such as magnetic null- and X-points (*e.g.* McLaughlin *et al.*, 2009), flux ropes (*e.g.* Kolotkov, Nisticò, and Nakariakov, 2016), and current sheets (*e.g.* Artemyev and Zimovets, 2012). Long QPPs with periods of several to tens of minutes are also detected as a broad band of solar flare emissions. They are commonly thought to be related with solar flare eruption in complex active regions or with the global oscillations of the Sun (Gelfreikh *et al.*, 1999; Shibasaki, 2001; O'Shea *et al.*, 2001; Ofman and Wang, 2002; Wang *et al.*, 2003; McAteer *et al.*, 2004; Gelfreikh, Nagovitsyn, and Nagovitsyna, 2006; Li and Gan, 2008; Tian *et al.*, 2015).

QPPs have attracted great attention in the solar physics literature because it is unclear which mechanisms cause them. Observations and simulations show that QPPs might be associated with fundamental physical processes in solar flares, such as energy release, magnetic reconnection, MHD waves, particle acceleration, and other kinetic effects (Nakariakov and Melnikov, 2009; Nakariakov and Zimovets, 2011). One mechanism may be able to successfully interpret the main characteristics in one event, but generally fails to explain all the features, with the result that the nature of QPPs is still not conclusively defined. If the mechanism were understood, then QPPs might be used to diagnose the physical parameters in the flaring region. Nakariakov *et al.* (1999) suggested that long QPPs could provide a remote diagnosis of solar plasma, assuming that QPPs are caused by kink or sausage waves in the flaring loops. Aschwanden *et al.* (1998) found that the shortest oscillation timescale is proportional to the flare loop radius, while it is inversely proportional to the trapped electron density in the loops detected from SXRs, indicating that a QPP is observational evidence of a periodic pumping of nonthermal electrons in a flaring loop, which is usually modulated by certain waves with various periods. Similar results are also reported in other articles (Nakajima *et al.*, 1983; Mangeney and Pick, 1989; Zhao, Mangeney, and Pick, 1991; Ning *et al.*, 2005; Asai *et al.*, 2001; Foullon *et al.*, 2005; Nakariakov *et al.*, 2006; Ofman and Sui, 2006; Li and Gan, 2008; Inglis and Dennis, 2012; Li, Ning, and Zhang, 2015a).

QPPs typically appear in multiwavelengths in the same event, which should help to understand the nature of the oscillation. The currently most frequently used instruments for

such studies include the *Geostationary Operational Environmental Satellites* (GOES), the *Atmospheric Imaging Assembly* (AIA) and the *Extreme Ultraviolet Variability Experiment* (EVE) onboard the *Solar Dynamics Observatory* (SDO), and the *Gamma Ray Burst Monitor* (GBM) onboard *Fermi*. In this article, we investigate QPPs in the 10 September 2014 flare that were detected by these instruments. The four-minute QPPs in this event have been well studied in several papers (Li and Zhang, 2014; Li, Ning, and Zhang, 2015a; Tian *et al.*, 2015). Different from the past studies, we investigate the one-minute QPPs in this event and present results that are independent of the past findings.

2. Observation and Measurement

The flare studied here is the X1.6 event on 10 September 2014. It started at 17:21 UT, reached its maximum at 17:45 UT, and ended at around 17:47 UT, according to GOES SXR observations. This event exhibits double ribbons in the chromosphere and a sigmoid structure in the corona, which is well detected by SDO/AIA (Lemen *et al.*, 2012). AIA has a pixel size of 0.60 arcsec and a time resolution of 24 s in 1600 Å and 1700 Å; the time resolution is 12 s at the other seven wavelengths of 304 Å, 211 Å, 193 Å, 131 Å, 171 Å, 94 Å, and 335 Å. Figure 1 shows a time sequence of flare images at five AIA wavelengths between 17:20 UT and 17:37 UT. There are two ribbons in the AIA 1600 Å image. The western flare (marked by Fpt_1 on the last AIA 335 Å image) is short around the positive magnetic polarity, and the eastern flare (marked by Fpt_2) is long; it looks like a circle around the negative polarity. This ribbon is more active and displays quasi-periodic knots (Li and Zhang, 2015; Li, Ning, and Zhang, 2015a; Zhang, Ji, and Su, 2016). The *Interface Region Imaging Spectrograph* (IRIS: De Pontieu *et al.*, 2014) slit is fixed on this ribbon to detect the whole development of this event. The flaring loops exhibit the sigmoid structure connection them, as shown in the AIA 131 Å images, and this structure brightens during the flare eruption.

Based on observations from SDO/AIA and IRIS, this solar flare has been well studied. For example, Li and Zhang (2015) found that some small-scale bright knots with redshifts at Si IV 1402 Å move along the flare ribbon with a quasi-period of 3–6 minutes, and the authors suggested that quasi-periodic slipping magnetic reconnection might be present in this flare. Combining this information with radio and HXR emissions, Li, Ning, and Zhang (2015a) found that the quasi-periodic knots are QPPs appearing over a broad wavelength range, with a period of exactly four minutes. Except for the intensity oscillations, the two chromospheric lines of Si IV and C I and the coronal line of Fe XXI also display similar oscillations in their line widths and redshifts. The authors have suggested that these QPPs could be caused by nonthermal electrons that are accelerated by quasi-periodic reconnection, which in turn is modulated by certain waves. Explosive chromospheric evaporation is found in this flare (Li, Ning, and Zhang, 2015b; Tian *et al.*, 2015), and the good correlation between the coronal line Fe XXI redshifts and HXR emission indicates that the nonthermal electrons can also simultaneously drive evaporation. Using the Grad–Rubin nonlinear force-free field extrapolation method, Zhao *et al.* (2016) found that the quasi-separatrix layer (QSL) footpoints match the observed flare ribbons very well during the rising phase. Cheng and Ding (2016) found that the magnetic flux rope (sigmoid structure) was comprised of different threads with different temperatures and densities, and that the flux rope caused a fast coronal mass ejection (CME) with a velocity of ≥ 1000 km s^{-1}, which further affected the solar wind density and speed at locations in the inner heliosphere (McKenna-Lawlor *et al.*, 2016). All these results are also confirmed by Dudík *et al.* (2016). Different from these articles, we
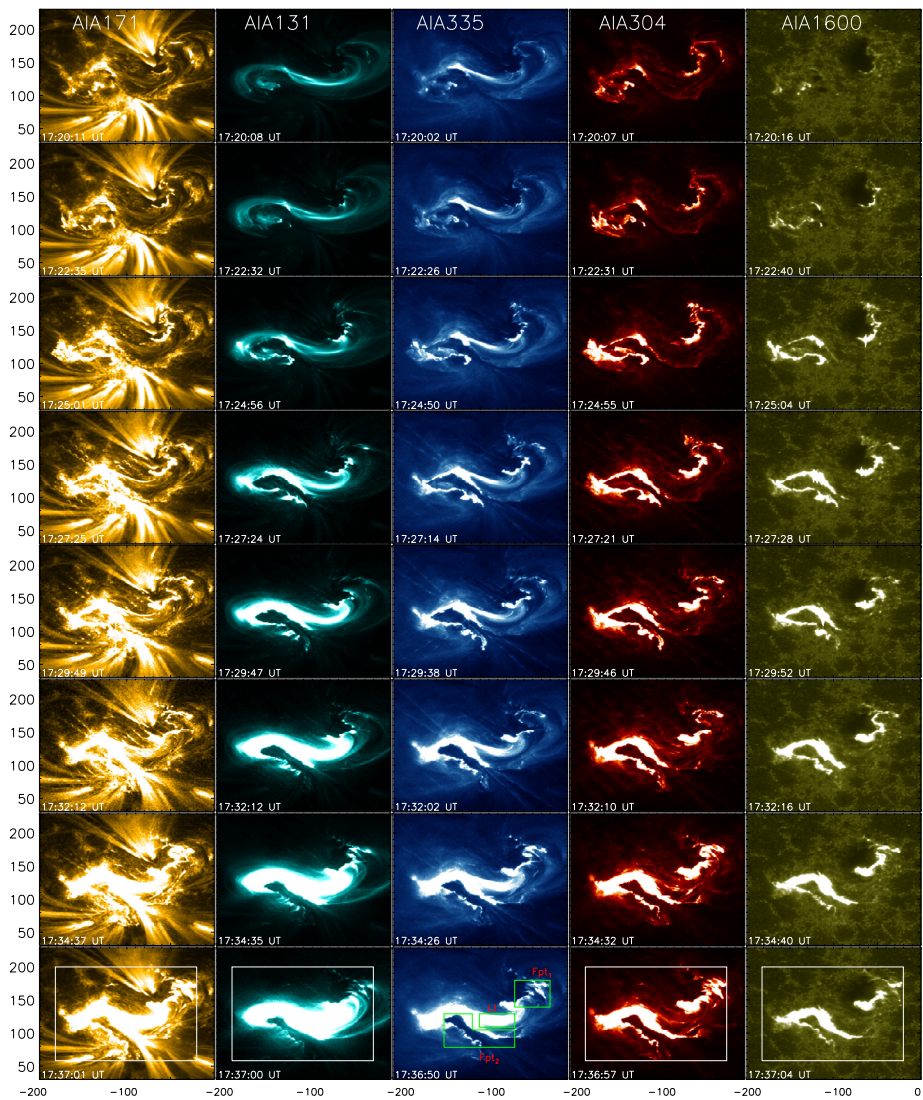
Figure 1 Time sequences of SDO/AIA maps at 171 Å, 131 Å, 335 Å, 304 Å, and 1600 Å between 17:20 UT and 17:37 UT. The flare loop footpoints (Fpt$_1$ and Fpt$_2$) and the loop top (Lt) are marked by three green boxes in the last AIA 335 image. The light curves in the white box are shown in Figure 4.

investigate the oscillations with a short period over a broad wavelength range; this is not studied or mentioned in these papers.

Figure 2 shows the GOES SXR light curve at 1–8 Å in the 10 September 2014 solar flare. Similar to a typical flare event, it displays an impulsive phase and a long decay phase. We detect the one-minute QPPs around the flare maximum. These QPPs exhibit a very small amplitude, with the result that they are hard to see on the original SXR light curve. The one-minute QPPs overlap with a strong background emission. In order to distinguish the one-minute QPPs from the background, we decompose the SXR light curve into a fast-
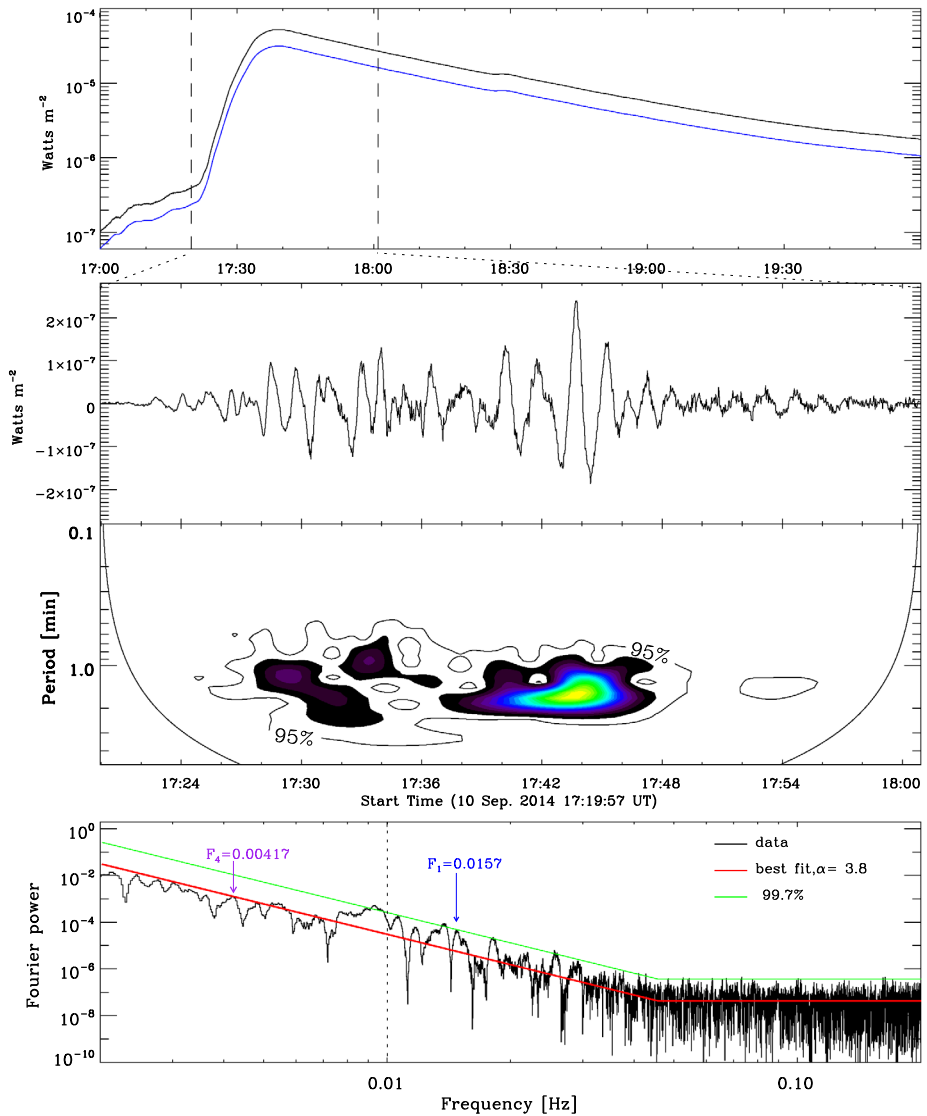
Figure 2 Upper panel: the light curve (black) of GOES SXR at $1-8$ Å and its slowly varying component (blue, after multiplying by 0.6) for the 10 September 2014 solar flare. Second and third panels: the fast-varying component in the interval between the two vertical dashed lines (upper panel) and its wavelet spectrum. Bottom: Fourier power of the GOES light curve, with the vertical dotted line marking the position (at the frequency of 0.01 Hz) that separates the domains of the fast- and slowly varying components. The red solid line is the best fit, and the green line shows the confidence level at 99.7 %. Two frequencies of 0.0157 Hz (about one minute) and 0.00417 Hz (about four minutes) are marked by blue and purple arrows, respectively.

varying component (second panel in Figure 2) and a slowly varying component (blue line in the top panel in Figure 2), which is multiplied by 0.6 to avoid overlap with the original light curve (black). To do this, we used the fast Fourier transform (FFT) method (Ning, 2014). First, the FFT power is calculated from the SXR light curves, as shown in Figure 2 (bottom).

Figure 3 Fourier power spectra of the fast-varying component in Figure 2 (second panel). The peak at 0.0157 Hz (about one minute) is marked by a blue arrow. The confidence level at 99.7 % is shown with the dotted line. Five other peaks above this level are also marked, and their frequencies are given.
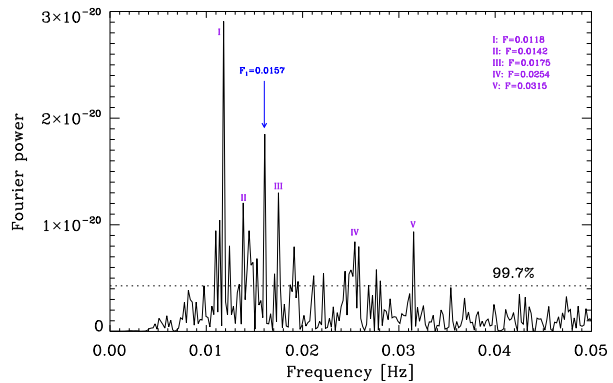
Similar to previous results (Vaughan, 2005, 2010; Dolla and Zhukov, 2011; Gruber *et al.*, 2011; Inglis, Ireland, and Dominique, 2015), the time series are dominated by a power law in the Fourier domain and a flat spectrum in the lower frequency region. In an astrophysical context, the former is often referred to as red noise (Vaughan, 2005), while the latter is white noise. The red noise is an intrinsic property of the physical system, and it is well described using a power-law model with a negative slope, *i.e.* $P(f) \simeq f^{-\alpha}$, where f is frequency. The best fit (red solid line) has $\alpha = 3.8$ for this flare. The blue line is parallel to the red line and represents the confidence level at 99.7 %. There are several subpeaks in the power-law spectrum, including a peak at 0.0157 Hz (about one minute, marked by the blue arrow) and 0.00417 Hz (about four minutes, marked by the purple arrow). These subpeaks reach but are not above the confidence limit, indicating that this flare does not seem to display any significant periodicity in the GOES SXR emission (Gruber *et al.*, 2011; Inglis, Ireland, and Dominique, 2015). However, the observations also show four-minute QPPs in this event (Li and Zhang 2014; Li, Ning, and Zhang, 2015a; Tian *et al.*, 2015). This contradiction might arise because the QPPs have small amplitudes. In order to identify QPPs with the short period of around one minute, the FFT power spectra are split into a lower and a higher frequency domain, as marked by the vertical dotted line at the separating frequency of 0.01 Hz. Finally, using the inverse FFT, the signals in the spectral domains are inverted into slowly varying (blue line in the upper panel) and fast-varying (second panel) components, respectively. The fast-varying component is the same as the original data minus the slowly varying component, which is similar to the residual emission subject to a simple moving average of 100 s. This results in the negative values in the fast-varying component. As mentioned before, the threshold period between these two components is arbitrarily chosen to be 100 s in this article. The GOES data have a time resolution of ≈ 2 s. Thus, the fast-varying component refers to fine structures with a timescale in the range of $2-100$ s, while the slowly varying component includes variations with a timescale longer than 100 s. Figure 2 (second panel) shows that the fast-varying component exhibits QPPs from the flare onset, *i.e.*, in the impulsive and maximum phases. The third panel gives the wavelet analysis of the QPPs between 17:20 UT and 18:00 UT, and the spectra show the period at around one minute, *i.e.* with a range from 50 s to 100 s. These QPPs change their amplitudes with time, and have a maximum value of 4×10^{-7} watts cm^{-2} at the flare peak at around 17:45 UT. This amplitude is about one percent of the SXR peak flux, which results in a weak peak in the FFT power spectrum of the GOES light curve. Figure 3 shows FFT power spectrum of the fast-varying component. The confidence level of 99.7 % is shown with the dotted line. There are more than six subpeaks above the confidence limit, as marked by
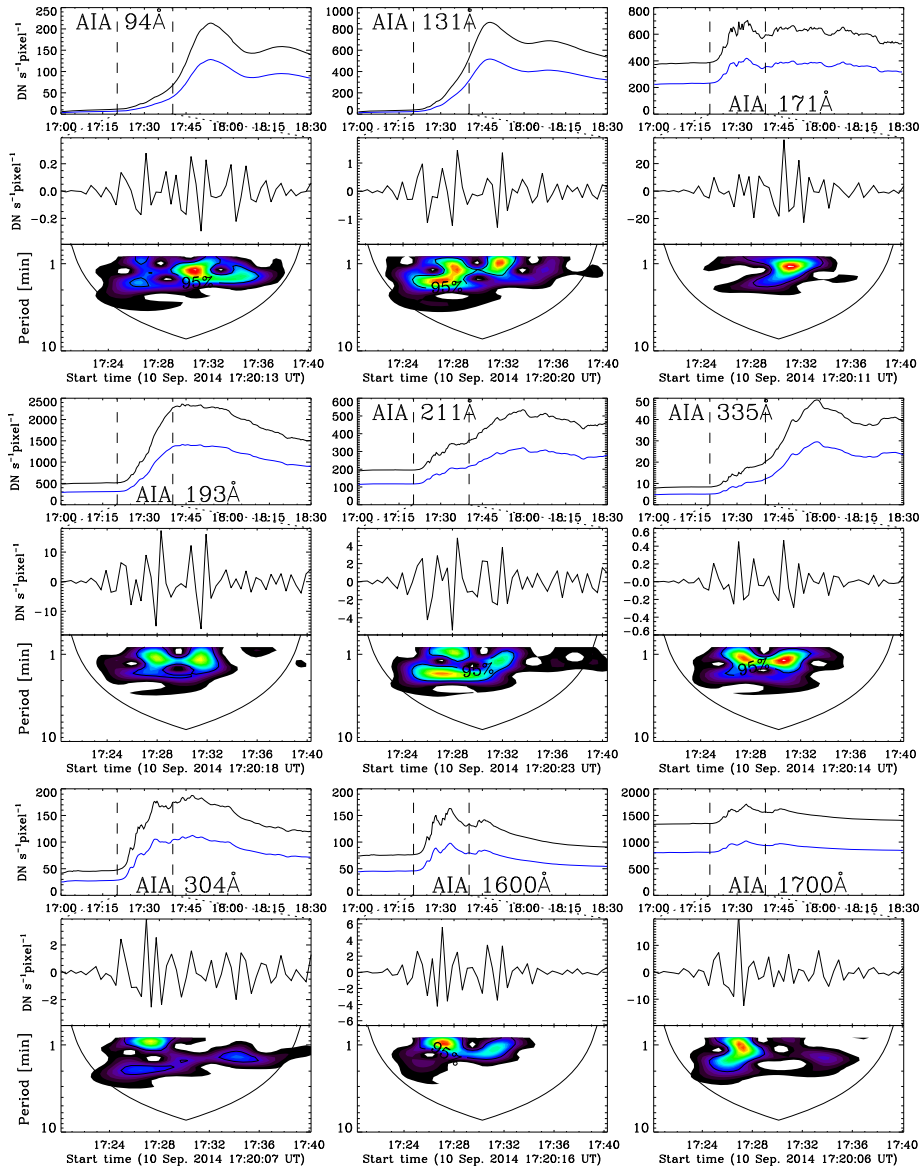
Figure 4 Following Figure 2, we show the light curves (black) of AIA 94 Å, 131 Å, 171 Å, 193 Å, 211 Å, 335 Å, 304 Å, 1600 Å, and 1700 Å, the slowly varying components (blue, after multiplying by 0.6), the fast-varying components, and their wavelet spectra.

roman numerals. They correspond to the period range from 31 s to 85 s. The blue arrow indicates the oscillation subpeak at exactly 0.0157 Hz (one minute).

Using the same method as for Figure 2, the one-minute QPPs are analyzed from the SDO/AIA observations. Figure 4 shows the light curves at nine AIA wavelengths (304 Å, 211 Å, 193 Å, 131 Å, 171 Å, 94 Å, 335 Å, 1600 Å, and 1700 Å), and the slowly (blue) and fast-varying components with their wavelet spectra between 17:20 UT and 17:40 UT.

AIA light curves are integrated over the whole flare region, as marked by the white box in Figure 1. They have here a time resolution of 24 s, not 12 s, to rule out the saturation images, which regularly appear after a normal image. As noted earlier, three steps are followed, and the threshold period is 100 s. The QPPs are identified in the fast-varying components for all nine AIA nine wavelengths, especially in the impulsive phase, *i.e.*, from 17:24 UT to 17:36 UT, after which the pulsation becomes weak, as shown in each bottom panel in Figure 4. The oscillation period is around one minute, *i.e.* a range from 48 s to 120 s. The oscillation amplitudes depend on the wavelengths, *i.e.*, the maximum value of 40 DN s^{-1} pixel^{-1} (which is about ten percent of the flare enhancement) in AIA 171 Å, and the minimum value of 0.4 DN s^{-1} pixel^{-1} in AIA 94 Å and 335 Å. Both wavelengths correspond to the plasma temperature in the coronal layer.

As well as AIA, the EVE (Woods *et al.*, 2012) data are also analyzed here. EVE has four EUV channels. The 18 nm (from 17.2 nm to 20.6 nm) waveband contains line emission that mainly comes from a thermal plasma around $1 - 2$ MK. The 26 nm (from 23.1 nm to 27.6 nm) and 30.4 nm (from 28.0 nm to 31.6 nm) channels mainly contain He II lines. The 36 nm channel is not used here due to some unknown problems. Similar to the GOES observations, SDO/EVE detects emissions from the whole Sun at a time cadence of 250 ms. Figure 5 shows the EVE data analysis. The light curves (black) of three channels are decomposed into slowly varying (blue) and fast-varying components. Their wavelet spectra are plotted between 17:20 UT and 18:00 UT. The pulsation is strong during this interval and becomes weak later, and the oscillation period is not exactly one minute, but around one minute, *i.e.* a range from 30 s to 120 s.

This event is also well observed by the GBM (Meegan *et al.*, 2009) onboard the *Fermi* space telescope. It has a continuous broad energy coverage (8 keV – 40 MeV) of the Earth unoccluded sky, and it consists of 12 Na I detectors ($8 - 1000$ keV) and two bismuth germanate detectors ($0.2 - 40$ MeV). The n2 (Na I) detector has a stable direction angle ($\approx 60°$) to the Sun during this event, especially in the interval from 17:10 UT to 17:45 UT. The other detectors change their direction angles frequently during the flare lifetime. After 17:45 UT, the n2 detector shifts its direction angle from $\approx 60°$ to $\approx 45°$ and then again to a higher value. The time resolution of Fermi is 0.256 s, but it becomes 0.064 s automatically in the flare state. Figure 6 (each top panel) plots the Fermi/GBM light curves in four energy bands, $4.6 - 12.0$ keV, $12.0 - 27.3$ keV, $27.3 - 50.9$ keV, and $50.9 - 102.3$ keV. Using the same method, these light curves are decomposed into slowly varying (blue) and fast-varying components. There are many subpeaks in the fast-varying component between 17:25 UT and 17:35 UT. The bottom panels give the wavelet spectra. The oscillation period is around one minute again, especially at $27.3 - 50.9$ keV. We interpolate all the data into a uniform resolution of 0.256 s. This cadence is enough to analyze the one-minute QPPs in this article. Li, Ning, and Zhang (2015a) found four-minute QPPs in this flare. Their separation period is 256 s (the authors used a smoothed window of 1000 points), and their slowly varying component has a period longer than 256 s. We use a separation period of 100 s here. In this case, the four-minute oscillation peaks are slowly varying components, such as the subpeaks at 17:25 UT, 17:29 UT and 17:33 UT in the blue lines at $27.3 - 50.9$ keV and $50.9 - 102.3$ keV shown in Figure 6.

3. Results

Using the FFT method, we identified the fast QPPs in the fast-varying components over a broad wavelength range observed by different instruments during the 10 September 2014
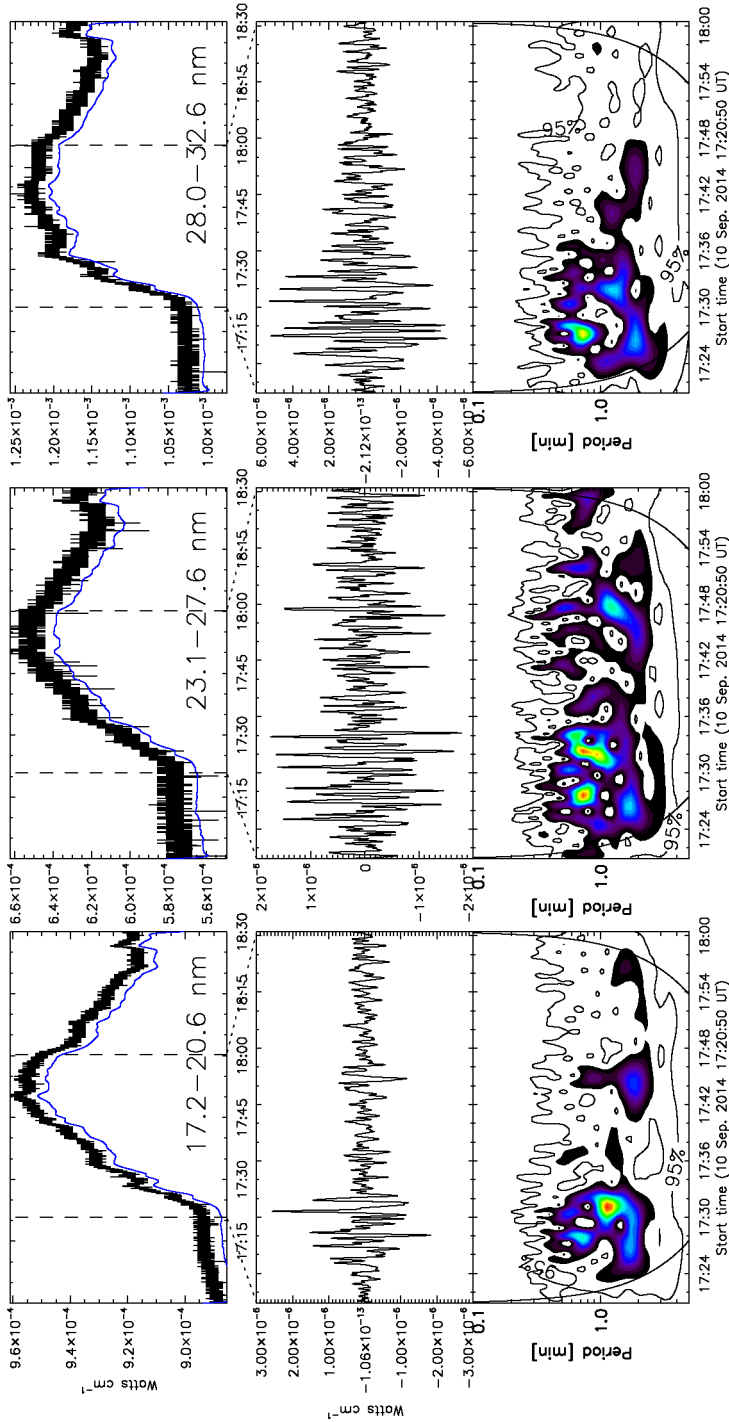
Figure 5 Following Figure 2, the light curves (black) from SDO/EVE, the slowly varying components, and their wavelet spectra at 17.2 – 20.6 nm, 23.1 – 27.6 nm, and 28.0 – 32.6 nm.
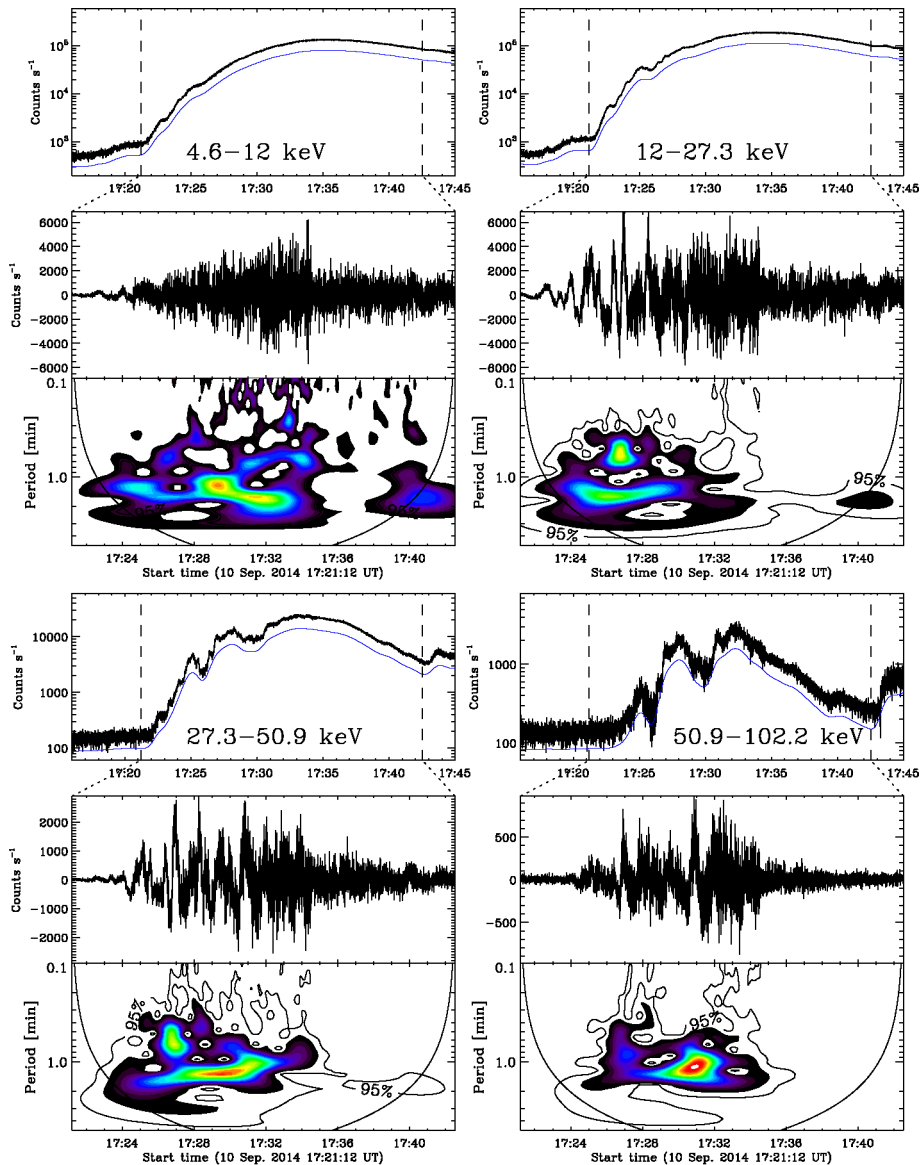
Figure 6 Following Figure 2, X-ray light curves (black) from Fermi at $4.6-12$ keV, $12-27.3$ keV, $27.3-50.9$ keV, and $50.9-102.2$ keV, the slowly varying components (blue, after multiplying by 0.6), the fast-varying components, and their wavelet spectra.

flare. The oscillation period is around one minute, *i.e.* in a range from 30 s to 120 s. Figure 7 plots the dependence of the fast-varying components of different wavelengths, *i.e.* AIA 94 Å versus other AIA wavelengths, Fermi $4-12$ keV versus GOES $1-8$ Å, and among the other three HXR channels. All the fast-varying components are positively correlated with each other. Although the correlations between Fermi $4-12$ keV and GOES $1-8$ Å and between AIA 211 Å and 94 Å have a coefficient lower than 0.5, the others have high correlation
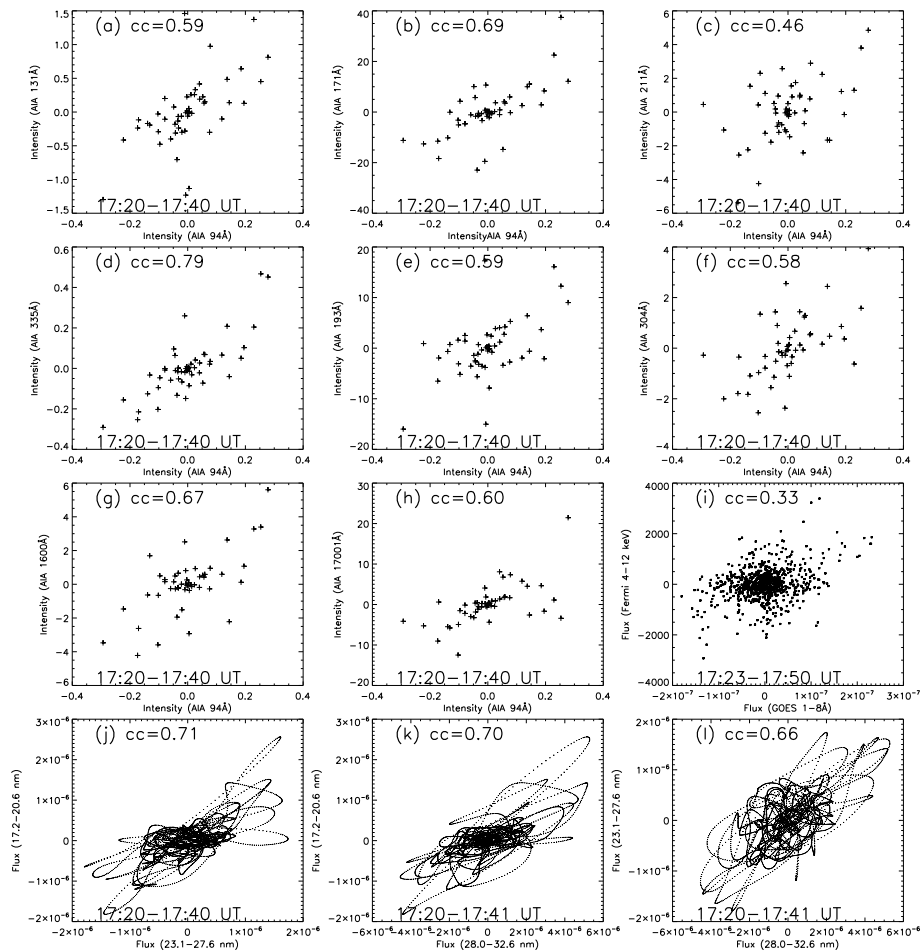
Figure 7 Correlation of various fast-varying components during the time interval between 17:20 and 17:40 UT, namely AIA 94 Å intensity dependence versus other wavelengths, and Fermi fluxes in 4–12 keV dependence versus GOES 1–8 Å, and EVE intensity dependence versus different wavelengths. The correlation coefficients (cc) are given.

coefficients (above 0.5), indicating that the one-minute QPPs really appear over a broadband of wavelengths simultaneously. Except for the correlation between Fermi 4–12 keV and GOES 1–8 Å, which is calculated after shifting the data by about 194 s, all other pairs of datasets in Figure 7 are plotted at exactly the same times. Figure 8 synthesizes the delay times or lags with respect to the reference channel in AIA 94 Å for other light curves whose correlation coefficients are maximal. All the channels exhibit their QPPs ahead of AIA 94 Å, except for the EVE 28.0–32.8 nm channel. This result is consistent with the standard thick-target flare model, in which precipitating nonthermal electrons bombard the footpoints of the flare loops (which radiate the HXR), which causes chromospheric evaporation. Evaporating hot plasma fills the coronal parts of flare loops and emits in different wavelengths, *i.e.* in SXR and EUV. Thus, it is expected that peaks of SXR and EUV emissions are delayed relative to peaks of HXR emission. The observed GOES (1–8 Å) and Fermi SXR (4.6–
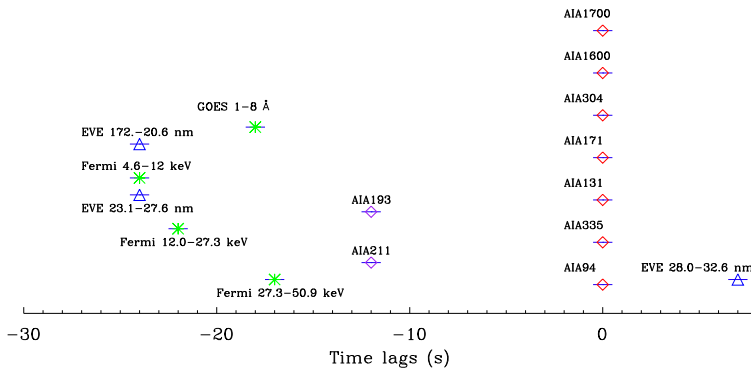
Figure 8   Time delays for the one-minute QPPs at various wavelengths (a negative delay means that the channel is ahead of the reference channel AIA 94 Å).
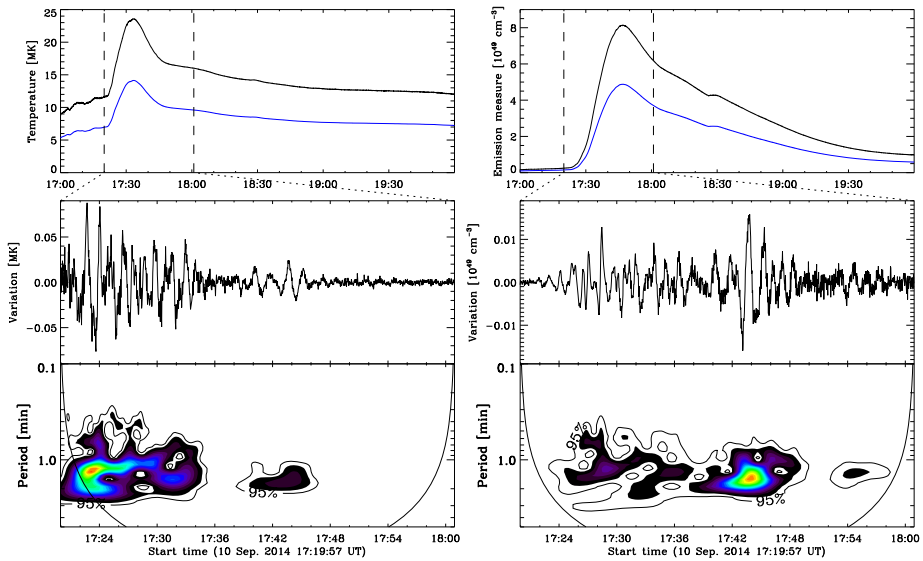

Figure 9   Following Figure 2, the time evolution of the plasma temperature and emission measure (black) detected from GOES data, the slowly varying components (blue, after multiplying by 0.6), the fast-varying components (middle), and their wavelet spectra (bottom).

12 keV) emissions are tens of seconds ahead of the Fermi HXR emission at $17.3 – 50.9$ keV. The reason might be that the HXR emission brightens later than the SXR emission, and the QPPs are detected in HXR later than in SXR. The maximum lag is about 30 s, *i.e.* between EVE $28.0 – 32.8$ nm and GOES $1 – 8$ Å or the other two EVE channels.

Figure 9 plots the one-minute QPPs at the plasma temperature and emission measure detected from the GOES data directly based on the thermal emission mechanism. Three steps are used to perform the analysis, as earlier. The time evolution of the plasma temperature and emission measure are decomposed into the slowly (blue) and fast-varying components (middle) with a separation period of 100 s. Wavelet spectra also display the QPPs with a period around one minute again between 17:20 UT and 17:50 UT. In contrast to the plasma

temperature, which displays the strong QPPs in the impulsive phase, the emission measure shows the strong QPPs around the SXR maximum phase.

4. Discussions and Conclusions

As well as the four-minute QPPs, the 10 September 2014 flare is found to exhibit one-minute QPPs in SXR, EUV, and HXR emissions. These QPPs are identified from the fast-varying components, which are identified in the light curves using the FFT method. The separation period is arbitrarily chosen to be 100 s, which is enough to rule out QPPs with a period longer than one minute. According to our method, the fast-varying component refers to variation with a timescale shorter than 100 s, while the slowly varying component refers to variation with a timescale longer than 100 s. In this case, the four-minute QPPs in this flare (Li and Zhang, 2015; Li, Ning, and Zhang, 2015a; Tian *et al.*, 2015) are the slowly varying components.

The wavelet and Fourier transform methods are used to analyze the period of the fast-varying components, and the results display an oscillation period of around one minute *i.e.* with a range from 30 s to 120 s. Fourier and wavelet spectra also show multiple strong narrow peaks (above the very high confidence level of 99.7 %) in the frequency range between ≈ 0.01 and ≈ 0.03 Hz. This fact indicates three possibilities: (1) the presence of multiperiod oscillations in the signal; (2) the 'quasi-period' varies in a broad range of $\approx 30 - 120$ s during the event, *i.e.* no persistent periodicity is present; (3) the time series used here are too short or sparse and the detected spectral peaks are the artificial result of the time-series analysis. The first two possibilities (1) and (2) are inherently similar and have previously been studied and discussed to some extent (*e.g.* Gruber *et al.*, 2011; Inglis, Ireland, and Dominique, 2015; Simões, Hudson, and Fletcher, 2015), but possibility (3) is ruled out because these pulsations are found in the light curves detected by various instruments. The Fourier spectral density of the GOES light curves shows small peaks of around one and four minutes in the power-law domain. The reason might be that the one-minute QPPs have a small amplitude, *i.e.* about one percent of the SXR peak flux, or ten percent of the flare enhancement in EUV. The one-minute QPPs have an amplitude of ≈ 4000 counts s^{-1} in Figure 6, about half of the four-minute oscillation amplitude (≈ 8000 counts s^{-1} from Figure 2 in Li, Ning, and Zhang, 2015a) in Fermi HXR at $27.3 - 50.9$ keV.

As mentioned, the 10 September 2014 flare simultaneously exhibits both one- and four-minute QPPs. It is interesting to investigate the spatial structure of the sources of one-minute pulsations using the SDO/AIA data and to compare this structure with the sources of the four-minute pulsation. Figure 1 shows a sigmoid structure connecting the double ribbons. It is possible that these pulsations with various periods originate from different flare regions. As a result, as we show in Figure 2, we detect the QPPs from the light curves at the two ribbons (marked by Fpt$_1$ and Fpt$_2$) and the sigmoid (Lt), as marked by the green boxes in the last AIA 335 Å image in Figure 1. The upper panels of Figure 10 show the AIA 335 Å light curves (black) from three regions, and blue lines are the slowly varying components. The lower panels show the fast-varying components. In contrast to the method shown in Figure 2, the separation threshold between two the components is chosen to be 300 s rather than 100 s in order to include both the one- and four-minute pulsations in the fast-varying component. The bottom panels show the Fourier spectra. Above the confidence level of 90 %, the four-minute pulsation peak is identified at the flare loop location and at the double footpoints, while the one-minute pulsation is only detected at the two footpoints. There is
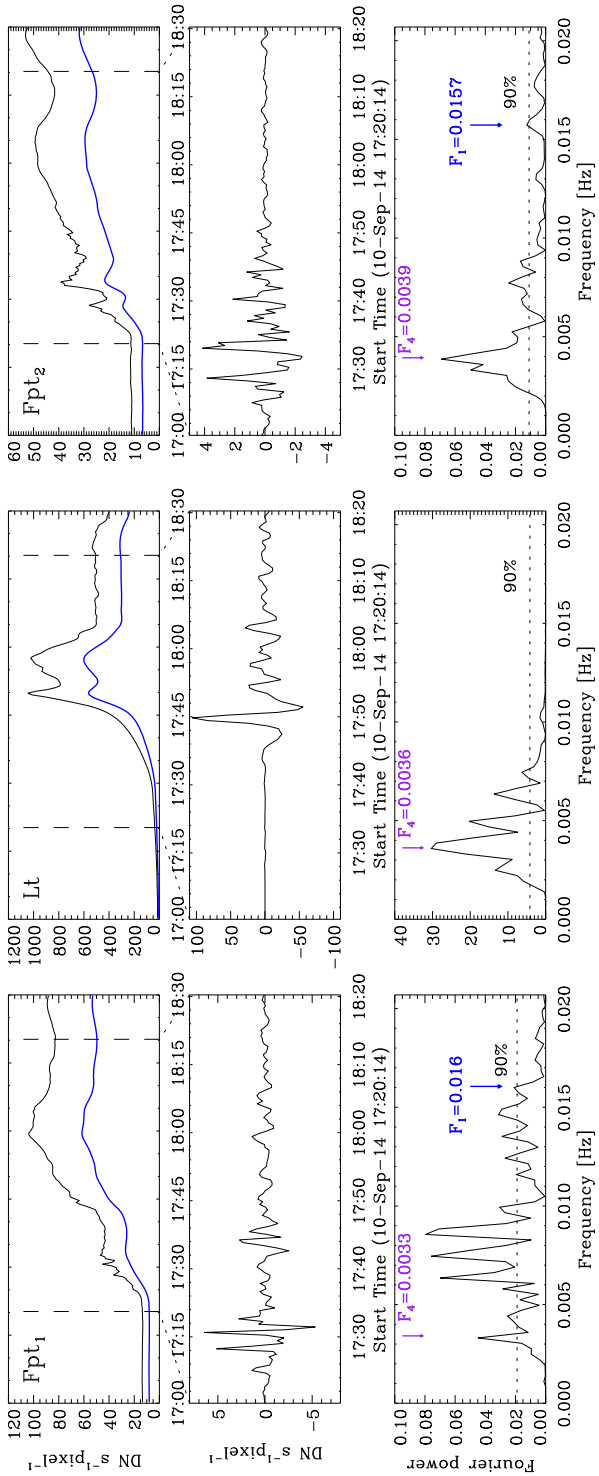
Figure 10 Upper panel: the light curve (black) of AIA 335 Å and its slowly varying component (blue, after multiplying by 0.6) at the regions around two footpoints (Fpt$_1$ and Fpt$_2$) and loop top (Lt), as marked by three green boxes in the AIA 335 image in Figure 1 (bottom). Second and third panels: the fast-varying component between the two vertical dashed lines (upper panel) and its Fourier power spectra. The confidence level at 90 % is shown with the dashed line. The arrows mark the typical frequencies of QPPs.
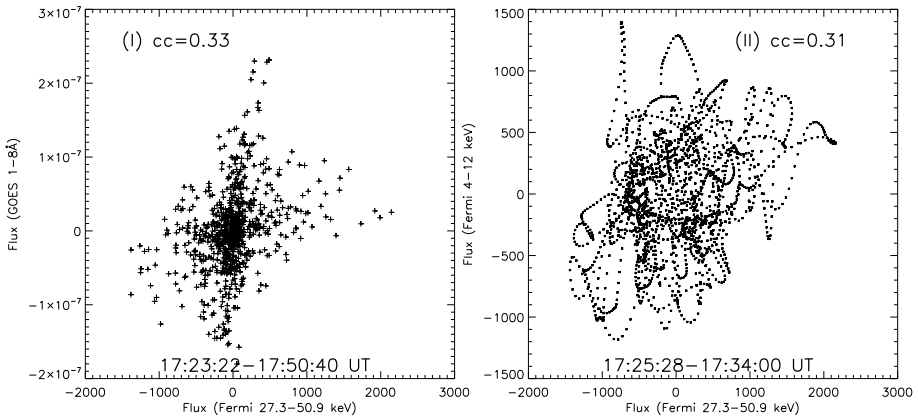
Figure 11 Correlation of the fast-varying components of GOES at $1-8$ Å and of Fermi at $4-12$ keV with those of Fermi at $27.3-50.9$ keV. The correlation coefficients (cc) are given.

no signal of a one-minute pulsation in the flare loop region (sigmoid). Meanwhile, the four-minute pulsations have stronger Fourier power than the one-minute pulsations.

The nature of the one-minute QPPs is still an open issue. The one-minute and four-minute pulsations both belong to the medium period of QPPs. Theoretically, there are two classes of interpretations for the middle QPPs in solar flares, such as periodic loading/unloading mechanisms of nonthermal electrons produced during the flare (*i.e.* an intrinsic property of the reconnection mechanism that leads to quasi-periodic behavior) or modulation of the electron beam or of parameters of the emitting plasma by MHD waves (Asai *et al.*, 2001; Fleishman, Bastian, and Gary, 2008; Inglis, Nakariakov, and Melnikov, 2008; Nakariakov and Melnikov, 2009; Nakariakov *et al.*, 2010b, 2016; Dolla *et al.*, 2012; Li *et al.*, 2014; Ning, 2014; Brosius and Daw, 2015). As noted earlier, the four-minute QPPs are detected in this event (Li and Zhang, 2015; Li, Ning, and Zhang, 2015a; Tian *et al.*, 2015). Li, Ning, and Zhang (2015a) found that four-minute QPPs appear in AIA light curves, type III radio bursts, and in HXR emissions. The four-minute QPPs have the same phase in the wide range from radio through UV to HXR emissions, indicating that the QPPs are possibly produced by nonthermal electrons accelerated by induced quasi-periodic reconnection or wave-modulation in the flare (Chen and Priest, 2006; Banerjee and Krishna Prasad, 2016). In this article, we also find one-minute QPPs in both the SXR and HXR emissions. Figure 11 plots the SXR intensity versus the HXR intensity, in particular the fast-varying components of GOES at $1-8$ Å and of Fermi at $4-12$ keV versus Fermi at $27.3-50.9$ keV. The data in $27.3-50.9$ keV are shifted by four seconds to achieve the maximum correlations here. Although the correlation is weak, the positive correlation suggests that one-minute QPPs might be caused by nonthermal electrons that are accelerated by wave-modulated reconnection. The pulsation periods could be the same as the period of the modulated waves. Namely, the magnetic reconnection might be simultaneously modulated by two different quasi-periodic processes. One process has a period of about four minutes, and the other has a period of around one minute in the 10 September 2014 flare. It is still an interesting question as to whether the one-minute oscillations are the fourth harmonic of the four-minute QPPs. This possibility is consistent with our finding that the spectral power of the four-minute pulsations is stronger than the power of the one-minute pulsations. In this case, it is also possible to detect the second (120 s), third (80 s),

fourth (60 s), fifth (45 s), sixth (40), etc. harmonics in the same event. Thus, there could be a range of characteristic timescales of the QPPs for an event, but no strong signature of a single period dominating in the power spectrum. On the other hand, Zimovets and Struminsky (2010) argued that doubly periodic X-ray emission could be a result of oscillations of two flare loop systems (Kupriyanova, Melnikov, and Shibasaki, 2013). It is not excluded that several different magnetic systems were present in the 10 September 2014 flare region, *i.e.* at least two, an eruptive S-shape magnetic flux rope, and surrounding loops (Cheng and Ding, 2016). Observations and simulations are needed to study flares that show QPPs with two or more quasi-periods in the future.

Disclosure of Potential Conflicts of Interest The authors declare that they have no conflicts of interest.

References

Artemyev, A., Zimovets, I.: 2012, *Solar Phys.* **277**, 283. DOI.

Asai, A., Shimojo, M., Isobe, H., Morimoto, T., Yokoyama, T., Shibasaki, K., Nakajima, H.: 2001, *Astrophys. J.* **562**, L103. DOI.

Aschwanden, M.J.: 1987, *Solar Phys.* **111**, 113. DOI.

Aschwanden, M.J., Benz, A.O., Dennis, B.R., Kundu, M.R.: 1994, *Astrophys. J. Suppl.* **90**, 631. DOI.

Aschwanden, M.J., Kliem, B., Schwarz, U., Kurths, J., Dennis, B.R., Schwartz, R.A.: 1998, *Astrophys. J.* **505**, 941. DOI.

Aschwanden, M.J., Kosugi, T., Hanaoka, Y., Nishio, M., Melrose, D.B.: 1999, *Astrophys. J.* **526**, 1026. DOI.

Banerjee, D., Krishna Prasad, S.: 2016, *MHD Waves in Coronal Holes*, *Washington DC American Geophysical Union Geophysical Monograph Series* **216**, 419. DOI.

Brosius, J.W., Daw, A.N.: 2015, *Astrophys. J.* **810**, 45. DOI.

Chen, P.F., Priest, E.R.: 2006, *Solar Phys.* **238**, 313. DOI.

Cheng, X., Ding, M.D.: 2016, *Astrophys. J. Suppl.* **225**, 16. DOI.

De Moortel, I., Ireland, J., Walsh, R.W., Hood, A.W.: 2002, *Solar Phys.* **209**, 61. DOI.

De Pontieu, B., Title, A.M., Lemen, J.R., Kushner, G.D., Akin, D.J., Allard, B., *et al.*: 2014, *Solar Phys.* **289**, 2733. DOI.

Dolla, L.R., Zhukov, A.N.: 2011, *Astrophys. J.* **730**, 113.

Dolla, L., Marqué, C., Seaton, D.B., Van Doorsselaere, T., Dominique, M., Berghmans, D., *et al.*: 2012, *Astrophys. J.* **749**, L16. DOI.

Dudík, J., Polito, V., Janvier, M., Mulay, S.M., Karlický, M., Aulanier, G., Del Zanna, G., Dzifčáková, E., Mason, H.E., Schmieder, B.: 2016, *Astrophys. J.* **823**, 41. DOI.

Fleishman, G.D., Bastian, T.S., Gary, D.E.: 2008, *Astrophys. J.* **684**, 1433. DOI.

Fleishman, G.D., Fu, Q.J., Huang, G.-L., Melnikov, V.F., Wang, M.: 2002, *Astron. Astrophys.* **385**, 671. DOI.

Foullon, C., Verwichte, E., Nakariakov, V.M., Fletcher, L.: 2005, *Astron. Astrophys.* **440**, L59. DOI.

Gelfreikh, G.B., Nagovitsyn, Y.A., Nagovitsyna, E.Y.: 2006, *Publ. Astron. Soc. Japan* **58**, 29. DOI.

Gelfreikh, G.B., Grechnev, V., Kosugi, T., Shibasaki, K.: 1999, *Solar Phys.* **185**, 177. DOI.

Gruber, D., Lachowicz, P., Bissaldi, E., Briggs, M.S., Connaughton, V., Greiner, J., van der Horst, A.J., Kanbach, G., Rau, A., Bhat, P.N., Diehl, R., von Kienlin, A., Kippen, R.M., Meegan, C.A., Paciesas, W.S., Preece, R.D., Wilson-Hodge, C.: 2011, *Astron. Astrophys.* **533**, A61. DOI.

Inglis, A.R., Ireland, J., Dominique, M.: 2015, *Astrophys. J.* **798**, 108. DOI.

Inglis, A.R., Dennis, B.R.: 2012, *Astrophys. J.* **748**, 139.

Inglis, A.R., Nakariakov, V.M., Melnikov, V.F.: 2008, *Astron. Astrophys.* **487**, 1147. DOI.

Karlický, M., Bárta, M., Mészárosová, H., Zlobec, P.: 2005, *Astron. Astrophys.* **432**, 705. DOI.

Kliem, B., Dammasch, I.E., Curdt, W., Wilhelm, K.: 2002, *Astrophys. J.* **568**, L61. DOI.

Kolotkov, D.Y., Nisticò, G., Nakariakov, V.M.: 2016, *Astron. Astrophys.* **590**, A120. DOI.

Kupriyanova, E.G., Melnikov, V.F., Shibasaki, K.: 2013, *Solar Phys.* **284**, 559. DOI.

Kupriyanova, E.G., Melnikov, V.F., Nakariakov, V.M., Shibasaki, K.: 2010, *Solar Phys.* **267**, 329. DOI.

Kupriyanova, E.G., Melnikov, V.F., Puzynya, V.M., Shibasaki, K., Ji, H.S.: 2014, *Astron. Rep.* **58**, 573. DOI.

Lemen, J.R., Title, A.M., Akin, D.J., Boerner, P.F., Chou, C., Drake, J.F., *et al.*: 2012, *Solar Phys.* **275**, 17. DOI.

Li, Y.P., Gan, W.Q.: 2008, *Solar Phys.* **247**, 77. DOI.

Li, D., Ning, Z.J., Zhang, Q.M.: 2015a, *Astrophys. J.* **807**, 72. DOI.

Li, D., Ning, Z.J., Zhang, Q.M.: 2015b, *Astrophys. J.* **813**, 59. DOI.

Li, T., Zhang, J.: 2014, *Astrophys. J.* **791**, L13.

Li, T., Zhang, J.: 2015, *Astrophys. J.* **804**, L8. DOI.

Li, B., Chen, S.-X., Xia, L.-D., Yu, H.: 2014, *Astron. Astrophys.* **568**, A31. DOI.

Mangeney, A., Pick, M.: 1989, *Astron. Astrophys.* **224**, 242.

McAteer, R.T.J., Gallagher, P.T., Bloomfield, D.S., Williams, D.R., Mathioudakis, M., Keenan, F.P.: 2004, *Astrophys. J.* **602**, 436. DOI.

McKenna-Lawlor, S., Ip, W., Jackson, B., Odstrcil, D., Nieminen, P., Evans, H., *et al.*: 2016, *Earth Moon Planets* **117**, 1. DOI.

McLaughlin, J.A., De Moortel, I., Hood, A.W., Brady, C.S.: 2009, *Astron. Astrophys.* **493**, 227. DOI.

Meegan, C., Lichti, G., Bhat, P.N., Bissaldi, E., Briggs, M.S., Connaughton, V., *et al.*: 2009, *Astrophys. J.* **702**, 791. DOI.

Nakajima, H., Kosugi, T., Kai, K., Enome, S.: 1983, *Nature* **305**, 292. DOI.

Nakariakov, V.M.: 2007, *Adv. Space Res.* **39**, 1804. DOI.

Nakariakov, V.M., Melnikov, V.F.: 2009, *Space Sci. Rev.149* 119. DOI.

Nakariakov, V.M., Zimovets, I.V.: 2011, *Astrophys. J.* **730**, L27. DOI.

Nakariakov, V.M., Ofman, L., Deluca, E.E., Roberts, B., Davila, J.M.: 1999, *Science* **285**, 862. DOI.

Nakariakov, V.M., Foullon, C., Verwichte, E., Young, N.P.: 2006, *Astron. Astrophys.* **452**, 343. DOI.

Nakariakov, V.M., Foullon, C., Myagkova, I.N., Inglis, A.R.: 2010a, *Astrophys. J.* **708**, L47. DOI.

Nakariakov, V.M., Inglis, A.R., Zimovets, I.V., Foullon, C., Verwichte, E., Sych, R., Myagkova, I.N.: 2010b, *Plasma Phys. Control. Fusion* **52**, 124009. DOI.

Nakariakov, V.M., Pilipenko, V., Heilig, B., Jelínek, P., Karlický, M., Klimushkin, D.Y., Kolotkov, D.Y., *et al.*: 2016, *Space Sci. Rev.* **200**, 75. DOI.

Ning, Z.: 2014, *Solar Phys.* **289**, 1239. DOI.

Ning, Z., Ding, M.D., Wu, H.A., Xu, F.Y., Meng, X.: 2005, *Astron. Astrophys.* **437**, 691. DOI.

Ning, Z., Wu, H., Xu, F., Meng, X.: 2007, *Solar Phys.* **242**, 101. DOI.

Ofman, L., Sui, L.: 2006, *Astrophys. J.* **644**, L149. DOI.

Ofman, L., Wang, T.: 2002, *Astrophys. J.* **580**, L85. DOI.

O'Shea, E., Banerjee, D., Doyle, J.G., Fleck, B., Murtagh, F.: 2001, *Astron. Astrophys.* **368**, 1095. DOI.

Shibasaki, K.: 2001, *Astrophys. J.* **550**, 1113. DOI.

Simões, P.J.A., Hudson, H.S., Fletcher, L.: 2015, *Solar Phys.* **290**, 3625. DOI.

Su, J.T., Liu, Y., Shen, Y.D., Liu, S., Mao, X.J.: 2012a, *Astrophys. J.* **760**, 82. DOI.

Su, J.T., Shen, Y.D., Liu, Y., Liu, Y., Mao, X.J.: 2012b, *Astrophys. J.* **755**, 113. DOI.

Sych, R., Nakariakov, V.M., Karlicky, M., Anfinogentov, S.: 2009, *Astron. Astrophys.* **505**, 791. DOI.

Tan, B.: 2010, *Astrophys. Space Sci.* **325**, 251. DOI.

Tian, H., Young, P.R., Reeves, K.K., Chen, B., Liu, W., McKillop, S.: 2015, *Astrophys. J.* **811**, 139. DOI.

Van Doorsselaere, T., De Groof, A., Zender, J., Berghmans, D., Goossens, M.: 2011, *Astrophys. J.* **740**, 90. DOI.

Vaughan, S.: 2005, *Astron. Astrophys.* **431**, 391. DOI.

Vaughan, S.: 2010, *Mon. Not. Roy. Astron. Soc.* **402**, 307. DOI.

Wang, T., Solanki, S.K., Curdt, W., Innes, D.E., Dammasch, I.E.: 2002, *Astrophys. J.* **574**, L101. DOI.

Wang, T.J., Solanki, S.K., Curdt, W., Innes, D.E., Dammasch, I.E., Kliem, B.: 2003, *Astron. Astrophys.* **406**, 1105. DOI.

Woods, T.N., Eparvier, F.G., Hock, R., Jones, A.R., Woodraska, D., Judge, D., *et al.*: 2012, *Solar Phys.* **275**, 115. DOI.

Yuan, D., Pascoe, D.J., Nakariakov, V.M., Li, B., Keppens, R.: 2015, *Astrophys. J.* **799**, 221. DOI.

Zhang, Q.M., Ji, H.S., Su, Y.N.: 2016, *Solar Phys.* **291**, 859. DOI.

Zhao, R.Y., Mangeney, A., Pick, M.: 1991, *Astron. Astrophys.* **241**, 183.

Zhao, J., Gilchrist, S.A., Aulanier, G., Schmieder, B., Pariat, E., Li, H.: 2016, *Astrophys. J.* **825**, 80. DOI.

Zimovets, I.V., Struminsky, A.B.: 2010, *Solar Phys.* **263**, 163. DOI.